Angular dependence of roughness-assisted surface plasmon radiation: Comparison of theory and experiment

D. G. Hall and A. J. Braundmeier, Jr.
Physics Department, Southern Illinois University, Edwardsville, Illinois 62026
(Received 9 May 1977)

We present a calculation of the angular distribution of surface-plasmon radiation from a rough surface. The radiated fields are calculated to first order in the surface-roughness height δ, and the results are compared with our earlier measurements. The present result is found to compare more favorably with experiment than a previous calculation by Kretschmann. The strength of the "backscattering" of surface plasmons from small surface features is determined and used to discuss certain features of the experimental results.

I. INTRODUCTION

A number of calculations of light scattering from rough surfaces have been reported recently. While not a complete list, Refs. 1–10 list a few of the important contributions. In an earlier paper,[11] we reported measurements of the angular distribution of the radiation emitted in the decay of surface plasmons at a rough silver surface. The geometry associated with that study is shown in Fig. 1(a). Surface plasmons, excited optically by the attentuated-total-reflection (ATR) method[12] at the air-silver interface, undergo radiative decay in the presence of surface roughness with intensity distribution $P(\theta)$. In what follows, θ is taken to be positive if measured clockwise, and negative if measured counterclockwise, from the normal (y axis) to the surface. The measurements were made for several samples and the results fell into three categories: (i) a single lobe in the $+\theta$ quadrant (forward direction), (ii) a lobe in the $+\theta$ quadrant along with a weaker lobe in the $-\theta$ quadrant (backward direction), and (iii) lobes of approximately equal intensity in the $+\theta$ and $-\theta$ quadrants. Figures 1(b)–1(d) show plots of intensity as a function of scattering angle θ for the three categories mentioned above. In Ref. 11, we pointed out that the growth of the radiation lobe in the $-\theta$ quadrant was always accompanied by a shift toward smaller values of θ of the peak in the forward direction. In this paper, we present the results of a calculation of the angular distribution $P(\theta)$ for a simple model of the scattering process. The results of the calculation are compared with our previous measurements as well as the results of an earlier calculation by Kretschmann.[13]

II. SCATTERING FROM A SINGLE DEFORMATION

To model the plasmon-roughness scattering process, we reduce the problem to two dimensions

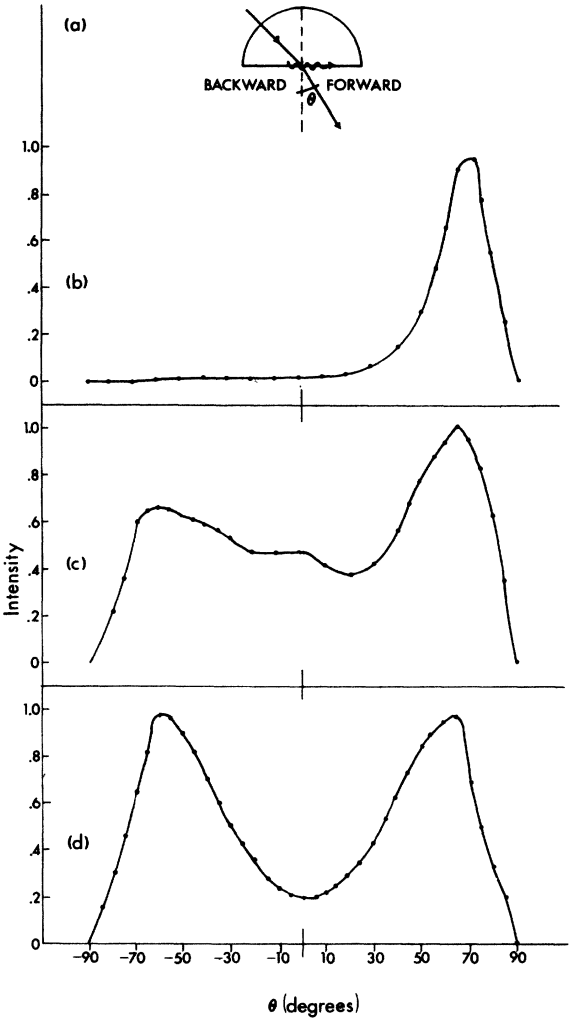

FIG. 1. (a) Geometry of the experiment in Ref. 11, defining the forward and backward directions relative to the direction of propagation of the surface plasmon; (b) single-lobed plasmon radiation pattern; (c) intermediate plasmon radiation pattern; (d) double-lobed plasmon radiation pattern.

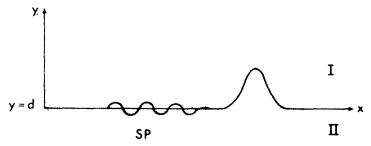

FIG. 2. Geometry of the surface-plasmon (SP) scattering calculation.

and consider the scattering of surface plasmons from a single surface deformation described by the function $f(x)$. The method used to calculate $P(\theta)$ is based upon the formalism developed by Chen[14] and applied to the problem of scattering a guided wave from a surface deformation by Tuan and Ou.[15] The technique (to be described below) can be applied to the problem of a surface plasmon scattered at the interface between two semi-infinite media (air and metal) or to the problem of a surface plasmon at one surface of a thin-metal film sandwiched between two semi-infinite dielectrics. The algebra associated with both problems is very similar, as is the resulting $P(\theta)$, and so we describe only the former in detail.

Figure 2 shows the geometry for the calculation. The (smooth) interface at $y = d$, separating media I and II, is interrupted by an irregularity described by the function $f(x)$. The height of the surface is given by the equation

$$y = d[1 + pf(x)], \tag{1}$$

where p is a small parameter related to the height of the bump on the surface, and the distance d from the origin to the surface is arbitrary. The incident surface plasmon (wavy line) is specified by the z component of the magnetic field (H_t) for surface plasmons propagating on a smooth surface ($y = d$) in the x direction

$$H_t^{\mathrm{I}}(x,y) = C \exp[-K_1(y-d)] \times \exp[-i(Kx - \omega t)], \quad y > d \tag{2}$$

and

$$H_t^{\mathrm{II}}(x,y) = C \exp[K_2(y-d)] \times \exp[-i(Kx - \omega t)], \quad y < d, \tag{3}$$

where

$$K_1 = [K^2 - (\omega/c)^2]^{1/2},$$

$$K_2 = [K^2 - \epsilon(\omega)(\omega/c)^2]^{1/2},$$

$\epsilon(\omega)$ is the dielectric function for the metal (medium II), K is the plasmon wave number, and C is a constant. The region above $y = d$ (medium I) is assumed to be vacuum.

The total field in each region of space will be given by the sum of two parts, the incident field plus the scattered field H_s. Under the assumption that H_s can be written as a power series in p, we write

$$H_s^{\mathrm{I}} = \sum_{n=1}^{\infty} p^n H_n^{\mathrm{I}} \tag{4}$$

and

$$H_s^{\mathrm{II}} = \sum_{n=1}^{\infty} p^n H_n^{\mathrm{II}}. \tag{5}$$

The boundary conditions on the fields are that the tangential component of the electric and magnetic fields are continuous across the boundary. The former can be written in terms of the gradient of the magnetic field

$$[\hat{n} \cdot \vec{\nabla}(H_t^{\mathrm{I}} + H_s^{\mathrm{I}})]_{\mathrm{I}} = \left(\frac{1}{\epsilon(\omega)} \hat{n} \cdot \vec{\nabla}(H_t^{\mathrm{II}} + H_s^{\mathrm{II}})\right)_{\mathrm{II}}, \tag{6}$$

where $\hat{n}$ is the outward normal to the surface and I and II represent, as before, air and metal, respectively. The latter boundary condition becomes

$$H_t^{\mathrm{I}} + H_s^{\mathrm{I}} = H_t^{\mathrm{II}} + H_s^{\mathrm{II}} \tag{7}$$

on the surface. Expanding Eq. (7) in a Taylor's series about $y = d$ and equating coefficients of equal powers of p gives (to first order)

$$H_t^{\mathrm{I}}(x,d) = H_t^{\mathrm{II}}(x,d) \tag{8}$$

and

$$H_1^{\mathrm{I}}(x,d) + df(x) \frac{\partial H_t(x,y)}{\partial y}\bigg|_{y=d} = H_t^{\mathrm{II}}(x,d) + df(x) \frac{\partial H_t^{\mathrm{II}}(x,y)}{\partial y}\bigg|_{y=d}. \tag{9}$$

To deal with Eq. (6), the operator $\hat{n} \cdot \vec{\nabla}$ must be expanded and written in terms of $f(x)$, the function describing the deformation of the surface (see Ref. 14). The operator takes the form

$$\hat{n} \cdot \vec{\nabla} = \left[1 + \left(pd \frac{\partial f(x)}{\partial x}\right)^2\right]^{-1/2} \times \left[\frac{\partial}{\partial y} - \left(pd \frac{\partial f(x)}{\partial x}\right) \frac{\partial}{\partial x}\right]. \tag{10}$$

Using Eq. (10) in Eq. (6), again expanding in a Taylor's series about $y = d$, and equating coefficients of equal powers of p results in (to first order)

$$\frac{\partial H_t^{\mathrm{I}}}{\partial y}\bigg|_{y=d} = \frac{1}{\epsilon(\omega)} \frac{\partial H_t^{\mathrm{II}}}{\partial y}\bigg|_{y=d} \tag{11}$$

and

$$\left.\frac{\partial H_1^{\mathrm{I}}(x,y)}{\partial y}\right|_{y=d} - d\,\frac{\partial f(x)}{\partial x}\left.\frac{\partial H_1^{\mathrm{I}}(x,y)}{\partial x}\right|_{y=d} + df(x)\left.\frac{\partial^2 H_1^{\mathrm{I}}(x,y)}{\partial y^2}\right|_{y=d}$$
$$= \frac{1}{\epsilon(\omega)}\left(\left.\frac{\partial H_1^{\mathrm{II}}(x,y)}{\partial y}\right|_{y=d} - d\,\frac{\partial f(x)}{\partial x}\left.\frac{\partial H_1^{\mathrm{II}}}{\partial x}\right|_{y=d} + df(x)\left.\frac{\partial^2 H_1^{\mathrm{II}}(x,y)}{\partial y^2}\right|_{y=d}\right). \quad (12)$$

Equations (8), (9), (11), and (12) can be combined to yield a pair of equations which describe the boundary conditions up to first order in p,

$$H_1^{\mathrm{I}}(x,d) - H_1^{\mathrm{II}}(x,d) = df(x)[\epsilon(\omega)-1] \times \left.\frac{\partial H_1^{\mathrm{I}}(x,y)}{\partial y}\right|_{y=d} \quad (13)$$

and

$$\left(\frac{\partial H_1^{\mathrm{I}}(x,y)}{\partial y} - \frac{1}{\epsilon(\omega)}\frac{\partial H_1^{\mathrm{II}}(x,y)}{\partial y}\right)_{y=d} = d\,\frac{\partial f(x)}{\partial x}\left(\frac{\partial H_1^{\mathrm{I}}(x,y)}{\partial x} - \frac{1}{\epsilon(\omega)}\frac{\partial H_1^{\mathrm{II}}(x,y)}{\partial x}\right)_{y=d} - df(x)\left(\frac{\partial^2 H_1^{\mathrm{I}}(x,y)}{\partial y^2} - \frac{1}{\epsilon(\omega)}\frac{\partial^2 H_1^{\mathrm{II}}(x,y)}{\partial y^2}\right)_{y=d}. \quad (14)$$

The right-hand side of Eqs. (13) and (14) can be evaluated using a specific form for $f(x)$ and the field expression given in Eqs. (1) and (2). For the sake of brevity, we define the right-hand side of Eqs. (13) and (14) by $M(x)$ and $N(x)$, respectively,

$$H_1^{\mathrm{I}}(x,d) - H_1^{\mathrm{II}}(x,d) = M(x) \quad (15)$$

and

$$\left.\frac{\partial H_1^{\mathrm{I}}(x,y)}{\partial y}\right|_{y=d} - \frac{1}{\epsilon(\omega)}\left.\frac{\partial H_1^{\mathrm{II}}(x,y)}{\partial y}\right|_{y=d} = N(x). \quad (16)$$

To determine the first-order scattered fields $H_1^{\mathrm{I}}(x,y)$ and $H_1^{\mathrm{II}}(x,y)$ subject to the above first-order boundary conditions, we follow Tuan and Ou[15] and use a Fourier-transform technique. We define the Fourier transform of $H_1^{\mathrm{I}}(x,y)$ and $H_1^{\mathrm{II}}(x,\ y)$ as

$$H_1^{\mathrm{I}}(x,y) = \left(\frac{1}{2\pi}\right)^2 \int\int_{-\infty}^{\infty} H_1^{\mathrm{I}}(\xi,\xi_1)\exp(-i\xi x) \times \exp[-i\xi_1(y-d)]\,d\xi\,d\xi_1, \quad (17)$$

and

$$H_1^{\mathrm{II}}(x,y) = \left(\frac{1}{2\pi}\right)^2 \int\int_{-\infty}^{\infty} H_1^{\mathrm{II}}(\xi,\xi_2)\exp(-i\xi x) \times \exp[-i\xi_2(y-d)]\,d\xi\,d\xi_2. \quad (18)$$

Similarly, the Fourier transforms of $M(x)$ and $N(x)$ are

$$M(\xi) = \int_{-\infty}^{\infty} M(x)\exp(i\xi x)\,dx \quad (19)$$

and

$$N(\xi) = \int_{-\infty}^{\infty} N(x)\exp(i\xi x)\,dx. \quad (20)$$

These may be used in conjunction with Eqs. (15) and (16) to give integral relations for $H_1^{\mathrm{I}}(x,y)$ and $H_1^{\mathrm{II}}(x,y)$,

$$H_1^{\mathrm{I}}(x,y) = \frac{1}{2\pi}\int_{-\infty}^{\infty} M(\xi)\exp(-i\xi x)\exp[-i\xi_1(y-d)]\,d\xi - \frac{i\epsilon(\omega)}{2\pi}\int_{-\infty}^{\infty}\left(\frac{N(\xi)+i\xi_1 M(\xi)}{\xi_2-\epsilon(\omega)\xi_1}\right)\exp(-i\xi x) \times \exp[-i\xi_1(y-d)]\,d\xi \quad (21)$$

and

$$H_1^{\mathrm{II}}(x,y) = -\frac{i\epsilon(\omega)}{2\pi}\int_{-\infty}^{\infty}\left(\frac{N(\xi)+\xi_1 M(\xi)}{\xi_2-\epsilon(\omega)\xi_1}\right) \times \exp(-i\xi x)\exp[-i\xi_2(y-d)]\,d\xi. \quad (22)$$

Since $H_1^{\mathrm{I}}(x,y)$ and $H_1^{\mathrm{II}}(x,y)$ satisfy the wave equations in their respective media, we have $\xi_1^2 = (\omega/c)^2 - \xi^2$ and $\xi_2^2 = \epsilon(\omega)(\omega/c)^2 - \xi^2$. The singularities in the integrals in Eqs. (21) and (22) can be shown to occur at the wave number

$$\xi = \pm(\omega/c)[\epsilon(\omega)/(\epsilon(\omega)+1)]^{1/2}, \quad (23)$$

which is the familiar surface plasmon dispersion relation for this geometry. The singularities correspond to surface waves reflected (+) and transmitted (−) at the surface irregularity.

To calculate the angular distribution of the radiation emitted into medium I (air), we solve Eq. (21) for $H_1^{\mathrm{I}}(x,y)$ far from the surface by the method of steepest descents.[16] As a specific example, we assume that $f(x)$ has the form of a Gaussian

$$f(x) = \exp[-(x/\sigma)^2], \quad (24)$$

with σ a parameter describing the width of the bump. With Eqs. (2) and (3), $M(x)$ and $N(x)$ become

$$M(x) = df(x)K_1 C[1-\epsilon(\omega)]\exp(-iKx) \quad (25)$$

and

$$N(x) = dC[1 - \epsilon(\omega)]\left(\frac{iK}{\epsilon(\omega)}\frac{\partial f(x)}{\partial x} - K_1^2 f(x)\right)\exp(-iKx). \tag{26}$$

Using Eq. (24), the Fourier transforms $M(\xi)$ and $N(\xi)$ are found to be

$$M(\xi) = \sigma\pi^{1/2}dCK_1[1 - \epsilon(\omega)]\exp[-\tfrac{1}{4}(K - \xi)^2\sigma^2] \tag{27}$$

and

$$N(\xi) = -\sigma\pi^{1/2}dC[1 - \epsilon(\omega)]\left(\frac{K^2 - K\xi}{\epsilon(\omega)} + K_1^2\right) \times \exp[-\tfrac{1}{4}(K - \xi)^2\sigma^2]. \tag{28}$$

Solving Eq. (21) and adopting a set of coordinates $y - d = \rho\cos\theta$ and $x = \rho\sin\theta$ gives the result

$$H_1^I(\rho, \theta) = \frac{k_0\cos\theta}{2\pi}\left[M(\xi) - i\epsilon(\omega)\left(\frac{N(\xi) + i\xi_1 M(\xi)}{\xi_2 - \epsilon(\omega)\xi_1}\right)\right] \times\left(\frac{2\pi}{k_0\rho}\right)^{1/2}\exp[-i(k_0\rho - \tfrac{1}{4}\pi)], \tag{29}$$

where $\xi = (\omega/c)\sin\theta$ and $\xi_1 = (\omega/c)\cos\theta$. The radiation patterns are obtained from $|pH_1^I(\rho, \theta)|^2$ normalized to the value at $\theta = \theta_{max}$, where θ_{max} is the angular position of maximum intensity.

A plot of the radiation patterns as determined from Eq. (29) for a Gaussian surface deformation shows $P(\theta)$ to be lobed in the forward direction. Adjusting the parameter σ serves only to shift the lobe's peak position and change the width of the lobe. In Fig. 3, we present a comparison of the calculated $P(\theta)$ with one of our measured angular distributions. The parameter σ has been chosen by requiring the peak position to be the same for both plots, in this case σ must be taken as 7000 Å. The dielectric constants chosen were those appropriate for silver[17] at $\lambda = 6328$ Å, $\mathrm{Re}[\epsilon(\omega)] = -16.64$ and $\mathrm{Im}[\epsilon(\omega)] = 0.52$. The agreement with experiment is quite good for the single-lobed distribution. Varying σ, the only adjustable parameter, does not lead to the growth of a second lobe in the backward direction. The forward-lobing characteristic of the calculated $P(\theta)$ does not appear to be strongly dependent upon the shape of the surface deformation. Another choice, such as a rectangular $f(x)$, also leads to a strongly forward-lobed $P(\theta)$. We have displayed the Gaussian lobed $P(\theta)$ because for the shapes we have tested it provides the best fit to experiment. The dependence of θ_{max} upon the value of σ for the Gaussian $f(x)$ is shown in Fig. 4. The peak position is quite sensitive to σ, allowing a precise value of σ to be assigned to the surface within the limits of this model.

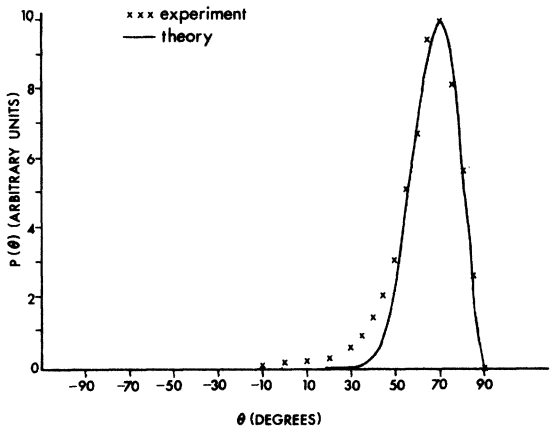

FIG. 3. Comparison of calculated (solid line) and measured (crosses) angular distribution $P(\theta)$ for single-lobed surface plasmon radiation pattern.

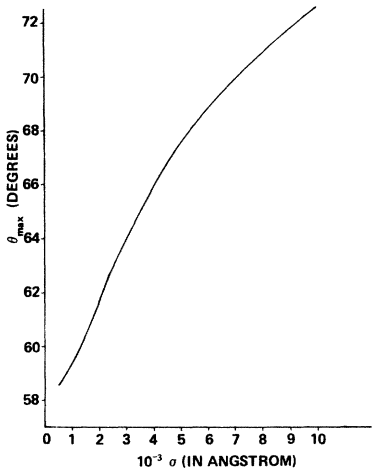

FIG. 4. Calculated dependence of θ_{max} [the angle at which $P(\theta)$ is a maximum] upon σ within the Gaussian model. θ_{max} is given in degrees and σ is given in 1000 Å units.

Kretschmann[13] has calculated $P(\theta)$ based on a model of radiating dipoles located (in air) at the air-metal interface. We find that there exists no value of σ, using a Gaussian autocorrelation function or any other reasonable choice, for which $P(\theta)$ determined from Kretschmann's calculation contains a lobe in the forward direction. We believe that the present calculation provides a more satisfactory description of the experimental results. It would appear that any slight deviation of a surface from planarity results in plasmon radiation in the forward direction. This is reasonable since a surface plasmon needs to reduce its momentum component parallel to the mean surface by only a very small amount to decay into a

photon. At the present time, we do not fully understand the origin of the discrepancy between Kretschmann's and our own result.

There remains the question of the origin of the plasmon radiation lobes in the backward direction. In our earlier paper,[11] we offered the suggestion that the mechanism responsible for these lobes is the scattering of surface plasmons from grain boundaries near the surface of the metal. That is, we postulated that a plasmon encountering a grain boundary would suffer appreciable "back reflection." The subsequent decay of the "back-reflected" wave would lead to a lobe in $P(\theta)$ in the backward direction. Referring once again to Fig. 1(a), the effect of grain boundaries is to produce surface waves traveling in both the $+x$ and $-x$ directions. Each will decay into photons (upon encountering small irregularities) contributing lobes in both the forward and backward directions. The formalism described herein allows us to calculate the level of "back reflection" to be expected from small surface irregularities. Equations (21) and (22) can be solved for the reflected fields by contour integration. The residues of these integrals corresponding to the poles at $\xi = +(\omega/c)(\epsilon/\epsilon+1)^{1/2}$ give the amplitudes of the reflected fields. The power associated with these fields is evaluated from the Poynting vector. When this is normalized to the incident power, the expression for the fraction of the incident energy carried by the wave reflected from a small Gaussian "bump" is

$$R = \pi \left| \frac{\delta K K_2 \sigma}{\epsilon(\omega)+1} \exp(-K^2\sigma^2) \right|^2 . \tag{30}$$

Differentiating Eq. (30) with respect to σ, we find that the value of σ which yields the maximum value of R is obtained from

$$\sigma^2 = 1/[2\,\mathrm{Re}(K^2)], \tag{31}$$

and is reminiscent of Bragg scattering. At $\lambda = 6328$ Å, R has a maximum value $R_{max} = (4.13 \times 10^{-3}$ Å$^{-2})\delta^2$. For realistic values of δ (say 10 Å), $R \approx 4 \times 10^{-4}$%. Even for $\delta = 1000$ Å, R_{max} is only 4%. We must conclude, then, that the back scattering of surface plasmons does not occur with appreciable intensity from small surface irregularities. This supports our suggestion of the grain-boundary mechanism. A grain boundary would very likely contribute to more severe scattering than a small "bump."

III. SCATTERING FROM SEVERAL DEFORMATIONS

The theoretical results of Sec. II are quite easily generalized to the case of more than one scattering center. We generalize the notation slightly, for convenience, and let δ be the average height of the irregularities, and δ_i be a height parameter such that the product $\delta\delta_i$ gives the height of the ith bump. The surface function is then given by

$$f(x) = \delta \sum_i \delta_i \exp\left[-\left(\frac{x - x_i}{\sigma_i} \right)^2 \right], \tag{32}$$

where σ_i is the width of the ith bump. The procedure of Sec. II gives, for the (unnormalized) radiation pattern $P(\theta)$,

$$P(\theta) = |F(\theta)|^2 \left| \sum_i \delta_i \sigma_i \exp[-i(\xi - K)x_i] \times \exp[-\tfrac{1}{4}(K-\xi)^2\sigma_i^2] \right|^2 , \tag{33}$$

where x_i is the location of the center of the ith scatterer

$$F(\theta) = \cos\theta \left[K_1 + i\left(\frac{K^2 - K\xi + \epsilon(\omega)K_1^2 - i\xi_1\epsilon(\omega)K_1}{\xi_2 - \epsilon(\omega)\xi_1} \right) \right], \tag{34}$$

and all other variables are as defined earlier. Similarly, R, the ratio of reflected to incident surface wave energies is given by

$$R = \pi\delta^2 \left| \frac{KK_2}{\epsilon(\omega)+1} \right|^2 \left| \sum_i \delta_i \sigma_i \exp(-i2Kx_i) \exp(-K^2\sigma_i^2) \right|^2 . \tag{35}$$

To be useful, Eqs. (33) and (35) must be averaged over the ensemble of scatterers. Defining $f(k)$ to be the Fourier transform of $f(x)$,

$$f(k) = \int_{-\infty}^{\infty} f(x) \exp(ikx)\, dx , \tag{36}$$

and letting $\langle \cdots \rangle$ represent the ensemble average, the (averaged) expressions in Eqs. (33) and (35) become

$$P(\theta) = (1/\pi)|F(\theta)|^2 \langle |f(K-\xi)|^2 \rangle \tag{37}$$

and

$$R = \delta^2 |KK_2/[\epsilon(\omega)+1]|^2 \langle |f(-2K)|^2 \rangle . \tag{38}$$

Some care should be taken in using Eqs. (37) and (38) because the form of $F(\theta)$, for example, depends upon the Gaussian choice for $f(x)$ given in Eq. (32).

The expression for the radiation pattern $P(\theta)$ given in Eq. (37) can be rewritten in terms of $g(k)$, the Fourier transform of the surface autocorrelation function. That is,

$$P(\theta) = (1/\pi)|F(\theta)|^2 g(K-\xi) . \tag{39}$$

If the random variables (δ_i, σ_i, and x_i) appearing in Eq. (32) are such that the standard assumption

of a Gaussian autocorrelation function is appropriate, then

$$g(K-\xi)=\pi\sigma^2\exp[-\tfrac{1}{4}(K-\xi)^2\sigma^2], \quad (40)$$

and $P(\theta)$ becomes identical to the results of Sec. II of this paper. That is, the Gaussian choice for $g(K-\xi)$ leads to a radiation pattern for the several-deformation problem which is the same as that for a single Gaussian-shaped scatterer with width equal to the parameter σ in $g(K-\xi)$ in Eq. (40).

IV. SUMMARY AND CONCLUSION

On the previous pages we have presented a calculation of the angular distribution of surface plasmon radiation. A comparison with experiment shows that the theory provides a very acceptable level of agreement for sample surfaces yielding a single scattering lobe in the forward direction. The calculation demonstrates that the interaction between surface plasmons and small scale surface roughness is not likely to produce lobes in $P(\theta)$ in the $-\theta$ quadrant. This is consistent with earlier work by Tuan and Ou[15] who found essentially the same result for the scattering of guided waves in a thin-film waveguide. The calculated results are consistent with our earlier suggestion[11] (made on empirical grounds) that the mechanism producing the lobes in the backward direction is the scattering of surface waves from grain boundaries near the surface of the sample. In particular, when the average separation between grain boundaries is a value which fulfills the Bragg condition, the back reflection of surface plasmons should be appreciable, contributing to a large lobe in the $-\theta$ quadrant.

It is clear that more detailed work is necessary before a completely satisfactory surface model can be found. Bennett[18] has recently reported the results of measurements of the surface autocorrelation function by scanning fringes-of-equal-chromatic-order (FECO) interferometry. Her measurements indicate that the usual assumption of a Gaussian autocorrelation function is not a particularly good one for the surfaces she examined. In fact, the autocorrelation function did not appear to have any simple form. Rasigni *et al.*[19] have recently reported measurements (using a different technique) of the surface autocorrelation function which indicate that a Lorentzian rather than Gaussian gives the best fit to their data. Our choice of a Gaussian form for $f(x)$ [see Eq. (24)] should not be viewed as being in conflict with Refs. 18 and 19. A Gaussian $f(x)$ does not necessarily imply a Gaussian autocorrelation function. In fact, it is possible to find a suitable arrangement of Gaussian shaped bumps on a sample which would yield virtually any kind of autocorrelation function. What is significant in this work is that the Gaussian shaped bump is the best choice of those functions we have tried for predicting the measured radiation patterns.

The calculation can certainly be improved upon by repeating the procedure allowing roughness in two dimensions rather than just one dimension. However, since the experiment[11] measured the photons emitted in the x-y plane, it is doubtful that this would have any effect upon the agreement reported in this paper. It would permit more general comparisons to be made with future experiments, and is therefore a desirable extension of the present work.

[1] P. Beckmann and A. Spizzichino, *Scattering of Electromagnetic Waves From Rough Surfaces* (Pergamon, Oxford, 1963).
[2] E. A. Stern, Phys. Rev. Lett. 19, 1321 (1967).
[3] E. Kroger and E. Kretschmann, Z. Phys. 237, 1 (1970).
[4] J. M. Elson and R. H. Ritchie, Phys. Rev. B 4, 4129 (1971).
[5] J. M. Elson and R. H. Ritchie, Phys. Status Solidi B 62, 461 (1974).
[6] J. M. Elson, Phys. Rev. B 12, 2541 (1975).
[7] A. Maradudin and D. L. Mills, Phys. Rev. B 11, 1392 (1975).
[8] V. Celli, A. Marvin, and F. Toigo, Phys. Rev. B 11, 1779 (1975).
[9] G. S. Agarwal, Opt. Commun. 14, 161 (1975).
[10] G. S. Agarwal, Phys. Rev. B 15, 2371 (1977).
[11] A. J. Braundmeier, Jr. and D. G. Hall, Surf. Sci. 49, 376 (1975).
[12] A. Otto, Z. Phys. 216, 389 (1968).
[13] E. Kretschmann, Opt. Commun. 5, 331 (1972).
[14] Y. M. Chen, J. Math. Phys. 9, 439 (1968).
[15] H. Tuan and C. Ou, J. Appl. Phys. 44, 5522 (1973).
[16] See, for example, R. E. Collin, *Field Theory of Guided Waves* (McGraw-Hill, New York, 1960), Chap. 11.
[17] L. G. Schulz, J. Opt. Soc. Am. 44, 357 (1954).
[18] J. M. Bennett, Appl. Opt. 15, 2705 (1976).
[19] M. Rasigni, G. Rasigni, C. T. Hua, and J. Pons, Opt. Lett. 1, 126 (1977).